Research Article

Characterization and dissolution behaviors of the Çatalağzı (Zonguldak, Turkey) power plant fly ash

Hatice YILMAZ*

Department of Mining Engineering, Faculty of Engineering, Dokuz Eylül University, İzmir, Turkey

Abstract: This study focused on the characterization and dissolution behaviors of fly ash produced by the Çatalağzı power plant (Zonguldak, Turkey) in which bituminous coal is burned. The fly ash, containing mainly a glassy phase and small crystalline phases, is a typical class F fly ash with pozzolanic properties. Therefore, it can be used in many different areas. For this material to be used safely, it is necessary to determine its dissolution behavior as well as its physical, chemical, mineralogical, and morphological properties. The dissolution behavior of the Çatalağzı power plant fly ash (CFA) was examined by two standard methods, namely TCLP 1311 and ASTM 3987 for some selected elements. Furthermore, the mineralogical and morphological changes in the CFA residues from dissolution processes were investigated using the XRD and SEM-EDS methods. The results obtained from characterization and dissolution tests showed that CFA can be considered as inert waste according to the EU waste acceptance criteria (EUWAC) limits and can be utilized as a raw material in many different sectors.

Key words: Çatalağzı fly ash, characteristics, trace element, dissolution tests, potential usage

1. Introduction

Coal has an important role in electricity production in Turkey as well as in the rest of the world. Although the fuel rankings vary over the years, coal is always in the top three in terms of electricity generation (EÜAŞ, 2021) in Turkey. The energy demand for Turkey has doubled in the last two decades, and this trend looks set to continue in the future with an average increase of 4% per year (Tanriverdi et al., 2021). In electricity generation, mainly lignite and bituminous coal, which are indigenous energy resources, are widely used in Turkey (EÜAŞ, 2021).

Turkey's only economic hard coal reserve of 1.3 Gt is located in the Zonguldak province in the western Black Sea Region; however, Turkey also has rich lignite reserves of 16 Gt with low calorific values scattered almost all over the country.[1] The calorific values of these reserves vary between 1000 and 5000 kcal/kg, and most (68%) have a low calorific value (<2000 kcal/kg). It is also defined as a fossil fuel with high ash, high moisture, high volatile matter, and high sulfur contents (Çapik et al., 2012; Tanriverdi et al., 2021). These low-calorific-value lignites can only be used for electricity generation in thermal power plants (Ediger et al., 2014; Oskay et al., 2013). Therefore, large volumes of fly ash are stored in dumping sites every year.

The properties of fly ash derived from coal depend on the characteristics of the feed coal, the combustion process, and the ash collection system (Jankowski et al., 2006, Medina et al., 2010; Akar et al., 2012). Fly ash becomes richer than coal in terms of its ash content (Vassilev et al., 2005; Goodarzi, 2006). Class F fly ashes have three major components which are silica, alumina, and ferrous compounds. Additionally, fly ash also contains minor oxides such as TiO_2, K_2O, Na_2O, CaO, and MgO and phosphorous oxides, as well as traces of Cu, Cr, Zn, Ni, and Mo oxides. Moreover, fly ash contains various toxic heavy metals such as Ni, Co, Cr, Cd, Zn, Mo, As, and Hg (Yadav and Fulekar, 2020). Besides these, rare earth elements and yttrium (REY) are enriched in both fly ash and bottom ash (Wang et al., 2019). So, fly ash obtained by burning coal is also an economically promising resource for the extraction of certain critical metals including Ge, Ga, REY, Nb, Zr, V, Re, Au, Ag, and base metals such as Al (Dai et al., 2016; Dai and Finkelman, 2018).

Fly ash poses a potential threat to developing countries, but it is not a serious concern for developed countries. This is because the fly ash utilization rate in some developed countries is higher than 90% (Yadav and Fulekar, 2020). In general, coal-derived fly ashes are used as raw material in some industries (e.g., cement and ceramic industries,

---

[1] EURACOAL (2022). Turkey/the voice coal of Europe [online]. Website https://euracoal.eu/library/archive/turkey/[accessed 19 01 2023].

* Correspondence: hatice.yilmaz@deu.edu.tr

building bricks) (Akar, 2001, Lee et al., 2008; Erol et al., 2008; Kizgut et al., 2010; Yildirim et al., 2011; Acar and Atalay, 2013; Tanriverdi et al., 2021; Roy et al., 2022), zeolite synthesis (Querol et al., 2001, 2002; Moreno et al., 2002; El-Naggar et al., 2008; Font et al., 2009; Akar et al., 2010; Panitchakarn et al., 2014; Top and Vapur, 2020), alumina and silica extraction (Moreno et al., 2002; El-Naggar et al., 2008; Font et al., 2009; Yilmaz and Karamahmut Mermer, 2016; Yadav and Fulekar, 2020), geopolymer production (Alvarez-Ayuso et al., 2008; Dwivedi and Jain, 2014; Atabey et al., 2020) and fly ash/sludge blend production for soil amendment (Wong, 1995; Veeresh et al., 2003; Seyrek, 2018).

Recently, there has been more and more research to utilize fly ash as an important raw material for REY recovery (Seredin and Dai, 2012; Hower et al., 2013, 2017, 2020, 2021; Franus et al., 2015; Kolker et al., 2017; Lin et al., 2017; Stuckman et al., 2018; Bielowicz et al., 2018; Dai and Finkelman, 2018; Huang et al., 2018, 2020; Wang et al., 2019; Żelazny et al., 2020; Rybak and Rybak, 2021; Hower and Groppo, 2021; Strzałkowska, 2022). There are also many studies about the possibilities of using some of the most valuable components of ash, i.e. microspheres, clay/shale, magnetic fractions, and nonmagnetic fractions of fly ash (Kolay and Singh, 2001; Vassilev et al., 2004; Lu et al., 2009; Kolay and Bhusal 2014; Żyrkowski et al., 2016; Strzałkowska and Adamczyk, 2019; Strzałkowska, 2021). As a result, pollution from fly ash can be a negative aspect, but the higher composition of valuable minerals such as silica, alumina, and iron and the recoverable rates of critical elements are some of the positive aspects of fly ash.

A comprehensive characterization of coal-derived fly ash is required to make the most of the positive aspects of fly ash. For this purpose, many characterization studies have been carried out on wastes produced by thermal power plants operating in Turkey (Egemen and Yurteri, 1996; Bayat, 1998; Akar, 2001; Baba and Kaya, 2004; Ugurlu, 2004; Karayigit et al., 2005; Erol et al., 2008; Akar et al., 2010; Baba et al., 2010; Haykiri-Acma et al., 2011; Yildirim et al., 2011; Acar, 2013; Karayiğit et al., 2019a, 2019b). In addition to the physical, chemical, mineralogical, and morphological properties of fly ash, its dissolution behavior is also extremely important (Liu et al., 2005; Jankowski et al., 2006; Jegadeesan et al., 2008; Akar et al., 2013; Yılmaz, 2015). The mobility of elements under different dissolution conditions, rather than their concentrations, is important in terms of their environmental risk assessments (Egemen and Yurteri, 1996).

The Çatalağzı power plant is the only power plant in Turkey that burns domestic hard coal. The coal that is burned in this plant consists of low-calorific-value residues of the beneficiation process of Upper Carboniferous hard coal from the Zonguldak Region. The mineralogical suite of the feeding coal consists mainly of clay minerals (kaolinite/chlorite and illite), secondary quartz, and minor amounts of calcite, dolomite, feldspar, and pyrite (Karayigit et al., 2000; Karayiğit et al., 2018). According to the chemical composition of the feeding coal, Si and Al are the main elements, while the contents of Fe, K, Na, Ca and Mg are at the levels of 0.05%–5%. Si is associated with quartz, clay minerals, and feldspar, and Al is associated with clay minerals and feldspar. Iron is associated with pyrite, and Ca and Mg are associated with carbonate minerals (calcite and dolomite) (Karayigit et al., 2000). The Çatalağzı power plant produces 300 MW (2 × 150) of electricity by burning 1.8 Mt/year of this coal, which has a calorific value of 13.79 MJ/kg (Kopac and Hilalci, 2007). The mineral content of 56% in the burned coal produces 0.65 Mt of ash per year, including bottom ash (20%) and fly ash (80%) (Kizgut et al., 2010).

Some studies have been carried out on the characterization and leaching behavior of fly ash of Çatalağzı power plant (Egemen and Yurteri,1996; Bayat, 1998; Acar, 2013; Acar and Atalay, 2013). However, in these studies, there have been some limitations in terms of the number of elements and method diversity. In this study, physical, chemical, thermal, mineralogical, and morphological characteristics of the Çatalağzı power plant fly ash (CFA) were determined. The results were evaluated in comparison to class F fly ashes of different countries and a standard class F fly ash (NBS 1633b certified). The dissolution behaviors of some selected elements (Al, Ag, As, Ba, Ca, Cd, Co, Cr, Cu, Fe, K, Mn, Mo, Ni, Pb, Sb, Se, Sr, Ti, and Zn) in the CFA were examined by using two different standard extraction methods (ASTM D-3987 and TCLP 1311). The obtained results were compared to the EUWAC (EU Council Decision 2003/33/EC) limits.

2. Materials and methods

2.1. Materials
The studied fly ash samples were collected every eight h for a week from the ESP discharge of the Çatalağzı power plant. The fly ash was divided by using a rotating sample splitter into approximately 100 g fractions and sealed in airtight bags for analyses and leaching tests. A representative sample was ground to minus 100 μm for chemical and mineralogical characterization.

2.2. Characterization methods
Bulk density and specific gravity were determined using a Micromeritics AccuPyc II 1340 gas Helium pycnometer. Particle size analyses were carried out using a Horiba LA-950 laser diffraction analyzer. Specific surface areas were determined using Quantachrome NovaWin2 equipment with multi-point BET measurements based on nitrogen adsorption. The thermal behaviors of the samples were determined by thermal treatment at three

different temperatures (750 °C, 1000 °C, and 1200 °C). Major element analyses were performed using an Analytic Jena NovAA 300 atomic absorption spectrometer (AAS) in fused lithium tetraborate ($Li_2B_4O_7$) solutions (Perkin Elmer, 1976) by using solid rock matrix reference materials (CRM). Trace element and leach solutions were analyzed using a Varian 710-ES inductively coupled plasma-optic emission spectrometer (ICP-OES) by using liquid pure 1000 ppm standard solutions (CRM) after the metal digestion and leaching processes, respectively. Qualitative and semiquantitative mineralogical analyses were performed using a Rigaku MiniFlex II XRD device by utilizing Cu Kα radiation filtered by a C monochromator. XRD patterns were obtained at 30 kV and 15 mA in a 2θ range of 3°–70°. XRD pattern analyses were performed by comparing the peak positions and intensities of the samples to the International Centre for Diffraction Data (ICDD) package program files. Morphological structural analyses and semiquantitative EDS analyses of the CFA fly ash and its leach residues were conducted using the SEM-EDS technique with a JEOL JXA-733 Superprobe.

2.3. Dissolution experiments
In this study, the USEPA-TCLP 1311 (1992) and ASTM D-3987 (2004) standard leaching procedures were applied. The ASTM D-3987 method is based on distilled water, while the TCLP method requires the determination of the appropriate solution depending on the natural pH value of the studied material. Therefore, the TCLP protocol was applied to determine the natural pH value of the CFA. First, 5.00 g of the dried sample was transferred to a 500 mL beaker, and 96.5 mL of distilled water was added. The beaker was covered with a watch glass and stirred vigorously using a magnetic stirrer for 5 min. The solution's pH was then measured. The pH was found to be higher than 5.0, 3.5 mL 1N HCl was added to the solution and stirred briefly, the mixture was covered with a watch glass and heated to 50 °C, and it was kept at 50 °C for 10 min. Then, the pH of the solution, which was cooled to room temperature, was measured as 5.0. According to the protocol, if the natural pH of the solution is below 5.0, TCLP extraction fluid #1 (acetic acid-NaOH buffer solution, pH: 4.98 ± 0.05) is used for the TCLP dissolution process; otherwise, for values over 5.0, TCLP extraction fluid #2 (unbuffered solution, pH: 2.88 ± 0.02) is used for the process. Since the natural pH of the CFA was determined as 5.0, the TCLP tests were

performed with extraction fluid #1 (pH: 4.98 ± 0.05). The TCLP test simulates the acidic condition, while the ASTM test simulates the normal aquatic condition. In both tests, the solid-to-liquid ratio was selected as 1: 20. After this, 50 g of the fly ash sample and 1 L of the appropriate leaching solution, as illustrated in standard methods, were added in 2-L polyurethane bottles and shaken for 18h. Leaching tests were performed on duplicate samples. After the leaching test suspensions were left to wait for 5 min, the final pH values of the solutions were measured. The leach solutions filtered with a 0.45-μm filter holder were acidified with HNO_3 to pH<2. These solutions were stored at 4 °C to prevent volumetric changes. The leach solutions were analyzed by ICP-OES for Al, Ag, As, Ba, Ca, Cd, Co, Cr, Cu, Fe, K, Mn, Mo, Ni, Pb, Sb, Se, Sr, Ti, and Zn. All measurements were made in duplicates, and the mean values were used.

3. Results
3.1. Characterization
3.1.1. Physical characterization
The physical and chemical properties of the CFA are given in Table 1. The CFA had a low specific gravity (2.18 g/cm³) and a high specific surface area (2.41 m²/g). The particle size distribution of the CFA was bimodal, with the first peak between 3 and 35 μm and a secondary peak between 35 and 450 μm (Figure 1). On average, 10% of the particles had a size smaller than 10 μm, and 10% of the material had a size greater than 147 μm, with a 50% particle size of 33 μm. Although a low specific gravity, a small particle size, and a high specific surface area are advantageous for industrial processes and chemical reactions (Sultana et al., 2011), they are disadvantageous for the mobility of trace elements, as well as the storage, conditioning, and disposal of fly ash.

3.1.2. Chemical characterization
The major and trace element concentrations of the CFA are given in Table 2. These results showed that the CFA had an aluminosilicate composition due to its high SiO_2 and Al_2O_3 contents. Its alkaline and alkaline-earth oxide contents (6.65%) were also very close to its Fe_2O_3 (6.37%) contents. Additionally, it contained TiO_2 (1.20 %) and SO_3 (0.72%), and its low loss on ignition (2.2% LOI) at high temperatures was probably due to the decomposition of carbonates and the combustion of unburned carbon.

Table 1. Some physical and chemical properties of the original CFA.

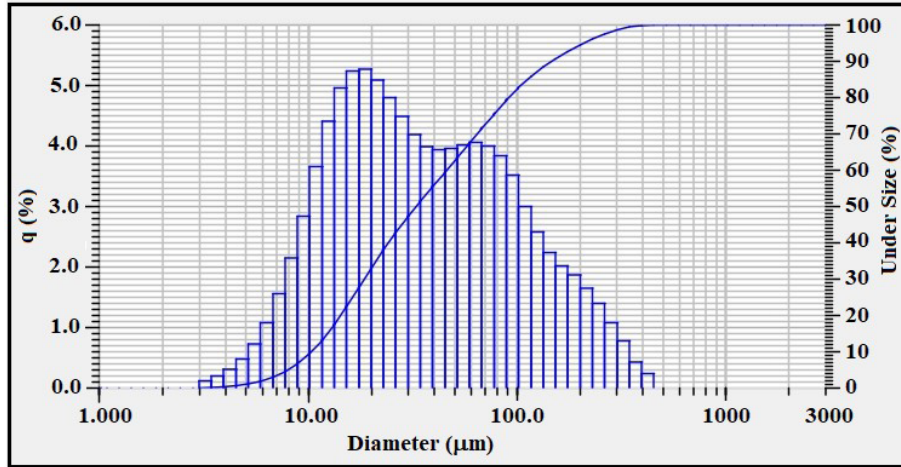| Mean size (μm)	Average particle size (μm)	Bulk density (g/cm³)	Specific gravity (g/cm³)	Specific surface area (m²/g)	Initial pH	Final pH TCLP	Final pH ASTM	LOI
68	33	0.81	2.18	2.41	9.05	5.13	10.04	2.23

Figure 1. Particle size distribution of the original CFA.

Table 2. Chemical composition of the original CFA (the results are reported according to the whole-fly ash basis dried at 105 °C in an oven).

Major Element (%)	CFA	Trace element (mg/kg)	CFA	Trace element (mg/kg)	CFA
SiO_2	58.70				
Al_2O_3	23.95	Ag	<0.05*	Mo	<0.05*
Fe_2O_3	6.37	As	32	Ni	73
CaO	0.80	Ba	150	Pb	<0.05*
MgO	2.18	Cd	2	Sb	<0.05*
Na_2O	0.39	Co	<0.05*	Se	<0.5*
K_2O	3.28	Cr	144	Sr	282
TiO_2	1.20	Cu	90	Zn	138
SO_3	0.72	Mn	588		
LOI	2.20	* below detection limit of the ICP-OES			

The trace element concentrations of fly ashes are important in terms of their environmental impact, and their usage as raw materials. In the CFA that was analyzed in this study, Sr, Mn, Cr, Zn, and Ba concentrations were above 100 mg/kg, while those of Cu, Ni, As, and Cd were under 100 mg/kg (Table 2). The silver, Co, Mo, Pb, Sb, and Se concentrations in CFA were below the detection limits of the ICP-OES. Therefore, the CFA contained siderophile (Ni, Cr, and Mn), lithophile (Ba and Sr), and chalcophile (As, Cd, Cu, and Zn) trace elements.

3.1.3. Mineralogy
It is not sufficient to characterize fly ashes based on chemical analysis alone, and this may even lead to erroneous results (Manz, 1999). Therefore, mineralogical analyses should be performed by considering the chemical compositions of fly ashes. The XRD pattern showing the mineralogical

composition of the CFA is illustrated in Figure 2. In this pattern, the low-intensity peaks indicate the low concentration of crystalline phases, while the high hump between 10° and 40° 2θ indicates the abundant presence of an amorphous phase. The amorphous phase consisted mainly of aluminosilicate glass (due to the abundance of silicon and aluminum) while the crystalline phases were composed mainly of mullite ($Al_6Si_2O_{13}$) and quartz (SiO_2), as well as minor amounts of calcite ($CaCO_3$), hematite (Fe_2O_3), and dolomite ($CaMg(CO_3)_2$). These results coincided with the conclusion that the mineralogical composition of the Çatalağzı power plant feeding coal (Karayigit et al., 2000; Karayiğit et al., 2018) consisted of illite, kaolinite/chlorite, quartz, feldspar, dolomite, calcite, and pyrite. Mullite crystallizes from the melting of aluminum silicate-based kaolinite and illite during

coal combustion (Spears, 2000; Dai et al., 2010). Similarly, hematite in the CFA was clearly formed mainly out of the oxidation of pyrite (Hu et al., 2006). Even though calcite is supposed to be decomposed during coal combustion, its presence in the studied fly ash sample could be related to partly reacted carbonate minerals or the carbonation of lime during the cooling of the fly ash (Fernandez-Turiel et al., 2004; Ji et al., 2019).

3.1.4. Thermal characterization
The DSC-TGA results of the CFA are illustrated in Figure 3. There are four weight loss regions in the TGA pattern. The initial weight loss (about 0.8%) was due to the removal of hygroscopic moisture between room temperature and 165 °C. The removal of the water of hydration at temperatures between 165 °C and 540 °C was accompanied by a weight loss of about 1.5%. A significant weight loss of about 0.5% was observed in the temperature range between 540 °C and 630 °C, mainly due to the decomposition of $CaCO_3$ and the combustion of the unburned coal contained in the fly ash. Finally, there was a weight loss of 1.7% at temperatures between 630 °C and 1000 °C. Thus, there was a total weight loss of 4.5%, including hygroscopic moisture, from room temperature to 1000 °C. The DSC pattern exhibits the presence of regular endothermic reactions up to 1000 °C, but no clear phase transformations.

Hence, three different temperatures (750 °C, 1000 °C, and 1200 °C) were applied to the CFA to further investigate the effects of thermal treatment on devitrification. The
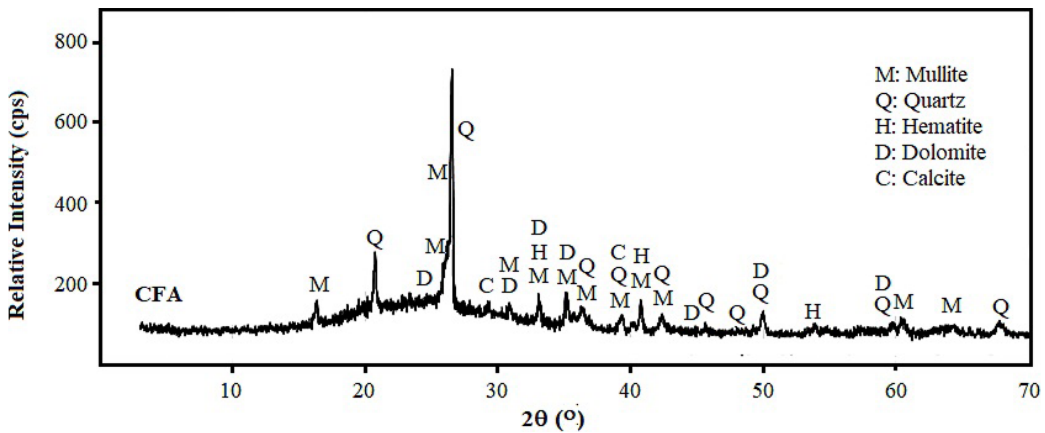

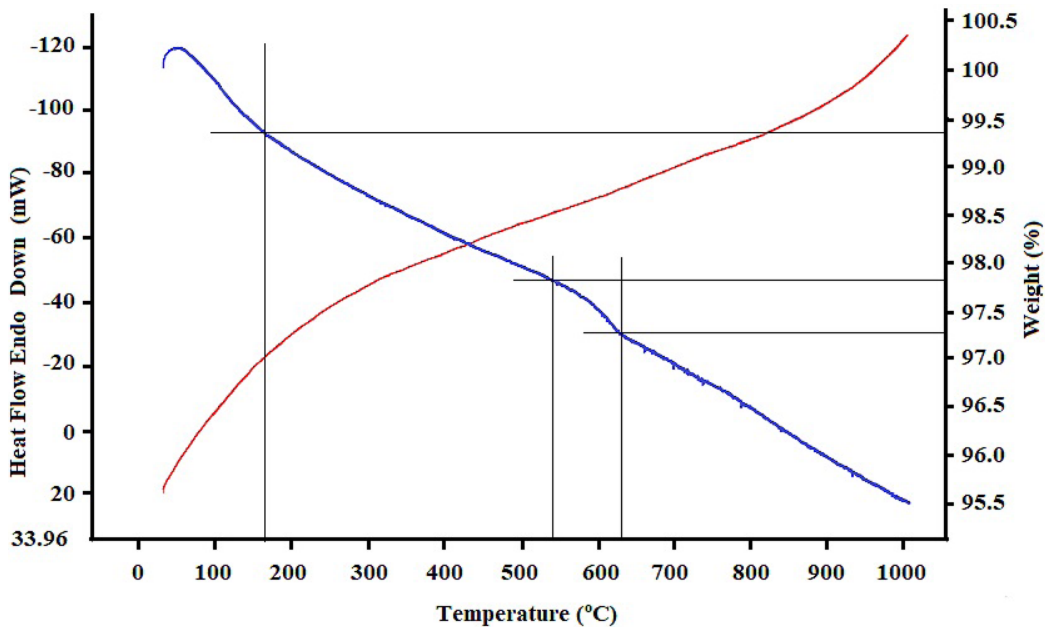**Figure 2.** XRD pattern of the original CFA sample.

Figure 3. DSC-TGA curves of the original CFA.

CFA sample lost 1.91% mass at 750 °C, 2.2% mass at 1000 °C, and 2.26% mass at 1200 °C, and it was sintered at 1200 °C. Then the mineralogical compositions of the treated CFA samples were examined and compared to the original CFA. Figure 4 shows the mineralogical changes of the CFA according to the thermal process. It is clear as seen in Figure 4 that the relative amounts of the crystalline phases of the CFA were changed by the thermal treatments that were applied. While the mullite and hematite contents increased along with the increasing temperature, the amounts of quartz decreased. Additionally, the calcite peak disappeared at 750 °C, and at 1000 °C, in addition to the calcite peak, the dolomite peak disappeared (Figure 4). The hercynite ($FeAl_2O_4$) phase appeared at 750 °C, and its relative concentrations increased along with the increasing temperature.

3.1.5. SEM and EDS analyses

Figure 5 shows the SEM images of the CFA sample at different magnification rates, and Table 3 exhibits the results of the semiquantitative SEM-EDS analyses of the selected grains in Figure 5. The SEM-BSE images reveal that the CFA sample was composed mainly of individual spherical particles (cenosphere) and minor partly agglomerated spherical and irregularly shaped particles at different sizes (Figures 5b–5f). Figure 5a shows free particles at a maximum size of 100 μm, while Figure 5f shows free particles at a minimum size of 0.1 μm. These results were in agreement with the particle size distributions (3–450

μm) in Figure 1. The SEM-EDS analyses showed that the spherical particles were composed of amorphous silica and/or different amorphous alkali aluminosilicate compositions. These results supported the XRD results in which a high hump pointed out a high amorphous phase. Figure 5b–2 shows a Ca-, K-, Al-, and Si-bearing amorphous cenosphere. Most of the spherical particles were composed of Mg-, Na-, and K-aluminosilicate (Figures 5b-1, 5d-3, and 5e-2), while lesser amounts of spherical particles were alkaline and alkaline-earth (Ca, Mg, Na, K) aluminosilicate (Figure 5d-2) in their compositions. Furthermore, unburned chars in fragmented particles were rarely observed (Figure 5c bottom right corner). The presence of crystalline phases such as lime (CaO) (Figure 5d-4), anhydrite ($CaSO_4$) (Figure 5d-1), and magnetite (Fe_3O_4) (Figure 5e-1), which could not be detected by the XRD method due to their low amounts, was also detected by SEM-EDS analysis as accessory phases. In the studied sample, lime, anhydrite, and magnetite were observed with characteristic cubic, orthorhombic, and octahedral structures, respectively. In particular, ferrospheres with dendritic magnetite crystallization are seen in Figures 5e-1 and 5f. Dendritic magnetite was formed as an incrustation on the surface of the amorphous silica and/or Ca-, Mg-, Na-, K-aluminosilicate spheres.

3.2. Dissolution behavior of CFA

The dissolution behavior of the CFA was investigated by two standard methods, namely ASTM and TCLP. While
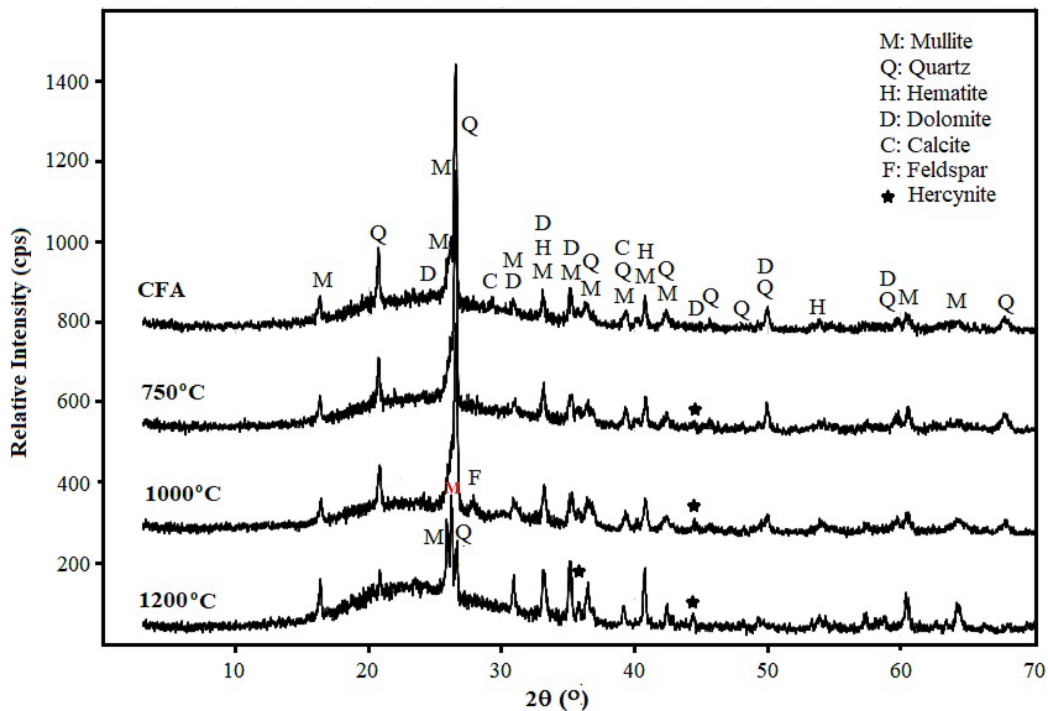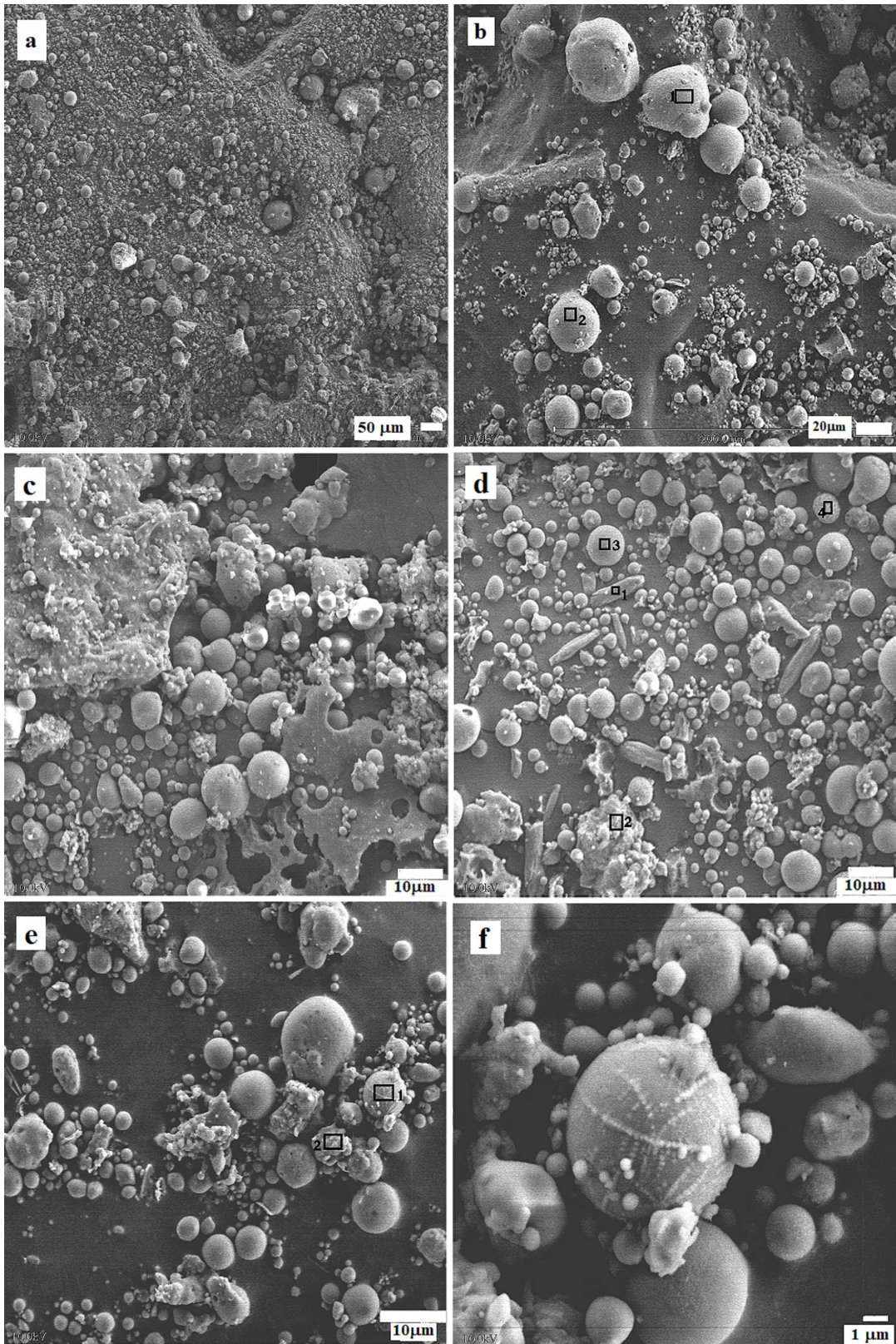

Figure 4. XRD patterns of the thermally treated samples and the original CFA.

Figure 5. Scanning electron microscopy (SEM) images of the original CFA. (5a–5e): SEM images at different magnification rates and EDS analysis positions of the CFA. (5f): Dendritic magnetite ferrosphere formed as an incrustation on the surface of the amorphous sphere.

Table 3. The results of semiquantitative SEM-EDS analyses on different particles of the original CFA whose positions are marked in Figure 5.

Element	Figure 5b		Figure 5d				Figure 5e	
	1	2	1	2	3	4	1	2
Si	30.42	25.47	3.67	18.84	29.65	10.28	18.17	27.14
Al	8.83	14.05	0.83	10.96	13.03	5.85	8.97	15.13
Fe	-	-	-	-	-	-	25.35	-
Ca	-	7.21	53.1	9.23	-	29.20	4.94	-
Mg	2.67	-	2.54	3.84	0.80	3.15	1.67	1.67
Na	3.29	-	-	4.53	2.34	7.24	1.95	3.18
K	7.3	7.25	3.87	10.87	4.1	6.92	5.25	3.54
S	2.05	1.64	8.22	2.70	3.36	4.17	1.27	2.75
O	45.42	44.38	27.78	39.01	46.71	33.17	32.46	46.58

distilled water was used as the dissolution medium in the ASTM method, the adjusted solution (pH: 4.98 ± 0.05) was used in the TCLP method. The initial pH value was 9.05 at the beginning of the ASTM method after the addition of distilled water, whereas the natural pH was 5.13 at the beginning of the TCLP method after the addition of the adjusted extraction fluid #1. The pH values of the ASTM and TCLP dissolution medium were constantly monitored and measured during the process. These values changed throughout the dissolution process and reached equilibria. The final pH values of the ASTM and TCLP test solutions were approximately 10.4 and 5.13, respectively, after 18 h of the dissolution process. Compared to the ASTM test medium, the TCLP test medium was highly acidic.

3.2.1. Dissolution of selected elements

At the end of the dissolution tests, the final pH was substantially lower for the TCLP method and a little higher for the ASTM method in comparison to the initial pH of 9.05. The increment in the pH value indicated the presence of soluble phases such as free Ca, soluble metal salts, oxides, hydroxides, and carbonates in the CFA.

Figure 6 shows the dissolution ratios of some selected elements, which were investigated in the CFA. Most of the elements, except As, leached at higher rates under the TCLP test conditions than under the ASTM test conditions. Arsenic is an oxyanionic element, and its leaching behavior is mainly dependent on pH. The solubility of As shows a maximum plateau around pH 7 to 11 (Izquierdo and Querol, 2012). Consequently, the leaching ratio of As was higher in ASTM (final pH ~ 10) than in TCLP (final pH ~ 5.1). Just like As, Cr is a cationic element, and its dissolution behavior is expected to be similar to that of As; however, its leaching behavior is quite different. In general, the lowest ratio of extraction occurs in neutral conditions for Cr. Nevertheless, its extraction is enhanced with increasing pH, and it forms a maximum plateau between pH 8 and 12. Additionally, the extraction ratio of Cr is high at pH values lower than 5.0 (Ecke et al., 2002; Zandi and Russell, 2007; Izquierdo and Querol, 2012). Consequently, the Cr extraction ratio in this study was slightly higher in the TCLP test conditions (pH 5.1) than in the ASTM (pH 10) test conditions.

Although Ca, Sr, K, and Ba had different extraction ratios, they showed similar leaching behaviors in both test conditions due to their high solubility. Magnesium displayed high solubility under the TCLP test conditions and low solubility under the ASTM test conditions. The solubility of Mg appears to be poor under acidic pH conditions, whereas it is insoluble in aquatic and alkaline conditions (Kim et al., 2003). This element has relatively low solubility, probably because it is enriched in the glassy phase of fly ash (Izquierdo and Querol, 2012). The dissolution ratios of the Mg in the CFA were 0.28% and 4.5% for the ASTM and the TCLP tests, respectively. The dissolution of Ca is also highly dependent on pH. Therefore, in this study, the dissolution ratio of Ca was 7.13% in the ASTM test, where the final pH was 10.04, while it was 44.51% in the TCLP test, where the final pH was 5.1. Potassium dissolved to almost equal extents under both the ASTM and the TCLP test conditions because soluble K in fly ash is in the form of Al-K-sulphate coatings that dissolve easily in aqueous environments (Izquierdo and Querol, 2012).

The dissolution of metallic ions (Mn, Ni, and Zn) only took place under acidic TCLP test conditions, and their extraction ratios were in the range of 0.5%–2%. However, these elements were insoluble in the case of the ASTM test conditions. This was because their leaching ratios are maximal in acidic conditions, whereas these ratios are minimal in the range of pH 8-10 and increase slightly over

pH 10, except for Ni, whose leaching ratio increases rapidly (Ecke et al., 2002; Zandi and Russell, 2007; Izquierdo and Querol, 2012). Cadmium and Cu are also metallic ions. However, their dissolution ratios were below the detection limits of the ICP-OES (<0.05 mg/kg) under both the ASTM and the TCLP test conditions. This situation can be explained by the very low concentration of Cd in the CFA (2 mg/kg) for Cd. Although copper had a high concentration in the CFA (90 mg/kg), its solubility was below the detection limit of the ICP-OES (<0.05 mg/kg) under both test conditions. Karayigit et al. (2018) revealed that chalcopyrite (CuFeS$_2$), a source of copper found in the coal burned in the Çatalağzı power plant, was related to illite. Since the glassy phase in fly ash is also formed by clay minerals in the feeding coal (Spears, 2004), copper in clay minerals accumulates in the glassy phase during the combustion process and cannot be easily dissolved from the glassy phase (Izquierdo and Querol, 2012). Similarly, Cu in the CFA was not readily dissolved under the ASTM and TCLP dissolution test conditions since it was in the glassy phase.

Titanium and Fe were not leached under both the ASTM and the TCLP test conditions. In the CFA, Fe was in the form of hematite and accessory magnetite which are extremely stable structures. They are not affected by acidic or basic environments; thus, Fe and other elements in these structures are not easy to dissolve. On the other hand, the source of Ti in fly ash is clay minerals and/or Ti-oxides in feeding coals (Karayigit et al., 2000; Karayiğit et al., 2018), which accumulate in the glassy phase during combustion. Therefore, the extraction behavior of Ti would be expected to be similar to that of Si, while in fact, Ti is an inert element and is insoluble at all pH values (Izquierdo and Querol, 2012).

3.2.2. Mineralogical characterization of the dissolution residues
Figure 7 comparatively exhibits the XRD patterns of the original CFA and its solid residues in the ASTM and TCLP dissolution tests. Mullite, quartz, calcite, dolomite, and hematite characteristic peaks are present on the original CFA pattern (Figure 2). These characteristic peaks were preserved in the pattern of the ASTM dissolution residue, whereas it is seen that all other peaks were in place, except for the calcite peak, in the pattern of the TCLP dissolution residue. As a result, only calcite was affected by the minerals in the CFA under the acidic TCLP test conditions, while no minerals were affected by the alkali ASTM test conditions. This was because all minerals except calcite are stable in an acidic environment; on the contrary, calcite can dissolve even in a weakly acidic environment. This also explains why Ca had a higher extraction ratio in the TCLP test (44.51%) than in the ASTM test (7.13%).

3.2.3. Morphological characterization of the dissolution residues
Figure 8 exhibits the morphological structures of the original CFA (Figures 8a and 8d) and its dissolution residues (Figures 8b, 8c, 8e, and 8f). The results show that there were some visual differences in some particles which were more pronounced in the TCLP test than in the ASTM test, and they are shown with yellow arrows in Figures 8e and 8f. It is observed that in the original CFA sample, there were intergranular linkages (indicated by yellow arrows in Figures 8a and 8d), while these linkages were largely absent in the TCLP residue (Figures 8b and 8c). This can be explained by the dissolution of the binding calcite under the acidic TCLP test conditions, which supported the finding that the element with the highest dissolution
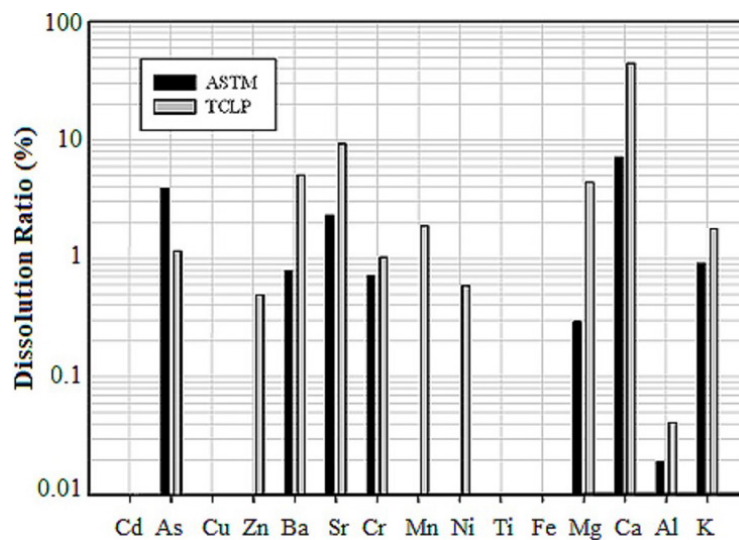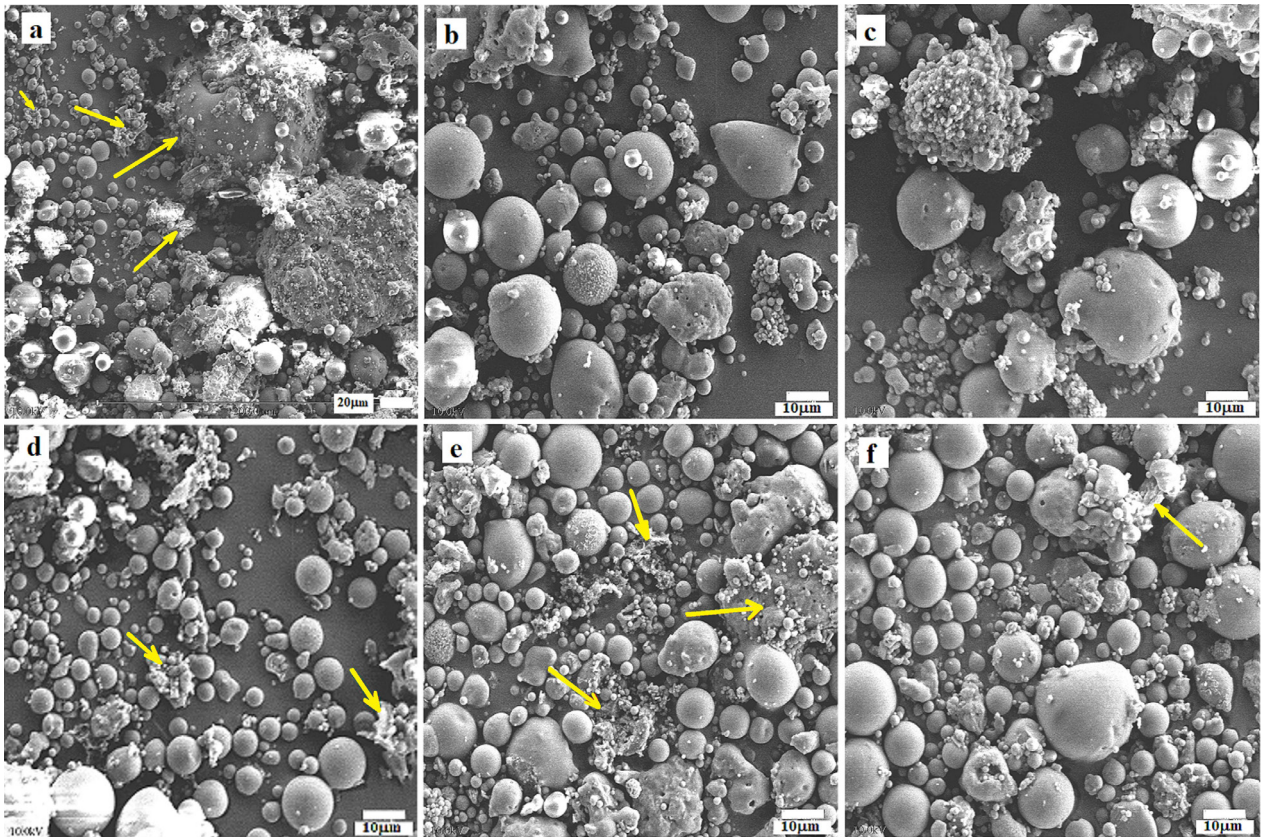

Figure 7. XRD patterns of ASTM and TCLP dissolution residue and the original CFA.

Figure 8. SEM images of the general view of the CFA and its dissolution residues. (a and d): Original CFA images, (b and c): TCLP residue images, and (e and f): ASTM residue images.

ratio in the TCLP test was Ca. The XRD examination of the solid residue of the TCLP test also revealed that the calcite peak was absent (Figure 7), while on the other hand, these linkages were observed in the ASTM residue (indicated by the yellow arrow in Figures 8e and 8f). This was also consistent with the fact that the binder calcite did not dissolve under the alkaline ASTM test conditions, and the dissolution ratio of Ca in the ASTM test was lower in comparison to that in the TCLP test (Figure 6). As a result, the calcite peak remained in place on the XRD pattern of the ASTM test solid residue (Figure 7).

The presence of linkages in the ASTM dissolution residue can also be explained by the normal distribution curves. So, the particle size distributions of the raw CFA, ASTM, and TCLP test solid residues were compared (Figure 9a). The plateau in the normal size distribution of the CFA (blue one) between 40 and 80 μm indicates that the proportions of the particles in this size range were almost equal. The plateau in the same region is slightly humped in the ASTM residue (red one), that is, there were some changes in the sizes of the particles. The same region also turned into a sharp peak in the TCLP residue. This can be explained by the dissolution of the binder calcite,

which held the grains together, the grains became free, and they formed a normal distribution. For the same reason, the normal distribution of the particles in the range of 10–40 μm shifted to smaller particle sizes. In total, the normal distribution curves for the small particles (<15 μm) shifted to smaller particle sizes for the TCLP residue compared to the ASTM residue (Figure 9b). This situation can be explained by the chemical dissolution of the calcite in the TCLP residue, as well as the mechanical effect influential in both samples at the end of the 18-h test periods.

4. Discussion

4.1. Chemical and mineralogical compositions
The chemical composition of the CFA is given in comparison to some class F fly ashes which were previously studied, such as European (23 fly ashes from pulverized coal-fired power plants of different European countries: Spain, Netherlands, Greece, and Italy), fly ashes from Spain (Moreno et al., 2005), Mexican fly ash (MFA) (Medina et al., 2010), Puertollano (Spain) fly ash, in particular (Moreno et al., 2005), Shubra El-Kheima (Egypt) fly ash (El-Naggar et al., 2008), and a certified fly ash NBS 1633b (international reference material) in Table 4. The CFA contained more than
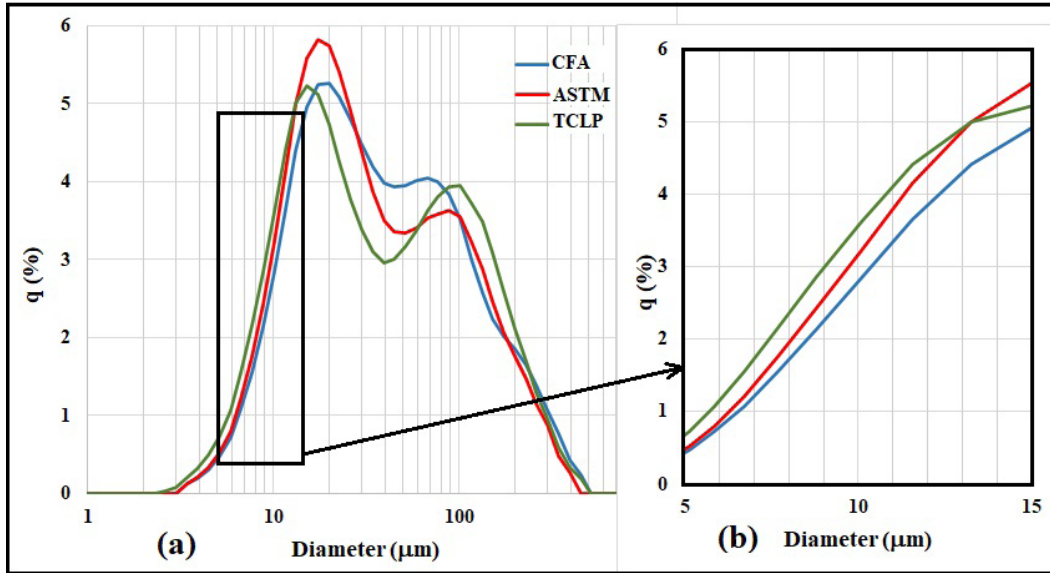
Figure 9. Normal distribution curves of the CFA, ASTM test residue, and TCLP test residue.

Table 4. The major element concentrations of the CFA and comparison to other fly ashes.

Elements (%)	CFA	NBS 1633b certified[a]	MFA[a]	European[b]	Puertollano Spain[b]	Shubra El-Kheima[c]
SiO_2	58.70	49.2	59.6	41.1–59.6	58.6	43.81
Al_2O_3	23.95	28.4	22.82	17.6–35.6	27.4	23.18
Fe_2O_3	6.37	11.1	5.57	2.6–16.0	7.3	0.01
CaO	0.80	2.1	3.11	0.5–11.8	0.8	6.10
MgO	2.18	0.8	0.87	0.8–3.8	1.0	0.80
Na_2O	0.39	0.3	0.45	0.1–1.2	0.3	0.87
K_2O	3.28	2.3	1.28	0.4–4.0	2.4	2.72
TiO_2	1.20	1.3	0.94	0.5–2.6	0.7	2.31
SO_3	0.72	0.5	0.4	0.1–8.6	0.2	15.68
Carbon	1.49	ND	5	0.6–7.6	0.7	-
SiO_2/Al_2O_3	2.45	1.73	2.61	1.2–2.8	2.1	1.88
Pozzolanic reactivity	89.02	88.8	88.00	74.5–93.3	93.3	67.00
TA-AE	6.65	5.5	5.71	1.8-20.8	4.5	14.99

[a] From Medina et al., (2010)
[b] From Moreno et al., (2005)
[c] From El-Naggar et al., (2008)
TA-AE: Total alkaline and alkaline Earth ($Na_2O+K_2O+CaO+MgO$)
ND: Nondetermined

70% SiO_2+Al_2O_3+Fe_2O_3 (total: 89.02%), and it had a high pozzolanic activity with low CaO (0.80%) and SO_3 (0.72%) contents. Additionally, the SiO_2/Al_2O_3 ratio (2.45%) of the CFA was also quite high. According to the ASTM C618 (1994) classification, the CFA can be classified as a class F fly ash. The pozzolanic activity of the CFA was almost equal to that of other fly ashes except for the Puertollano fly ash. Besides, the SiO_2/Al_2O_3 ratio of the CFA was higher than those of other fly ashes (except for MFA).

The XRD analyses (Figure 2) showed that the CFA had a highly amorphous structure and contained low amounts of crystalline phases consisting predominantly of mullite

and quartz, as well as minute amounts of calcite, hematite, and dolomite. Furthermore, the SEM-EDS analyses (Figure 5 and Table 3) showed that the amorphous glassy phase of the CFA was mainly alkaline and alkaline-earth aluminosilicates in the form of cenospheres, irregularly shaped particles, and agglomerates with complex structures.

The total alkaline and alkaline-earth (TA-AE) content of the CFA (6.65%) was low (Table 4), and some of them were used in the formation of crystalline phases (calcite, dolomite). In particular, K_2O was not used in the formation of any crystal phase, and not all of the MgO was consumed in the formation of dolomite. If it were, a more pronounced dolomite peak should have been observed. Therefore, all the K_2O and a significant part of the MgO would be in the amorphous glassy phase. Although mullite and quartz were the main crystalline phases in the CFA, their proportions would also consume a limited part of the Al_2O_3 and SiO_2 in the CFA, and the remainder would form the abundant aluminosilicate glassy phase. In addition, some of the Fe_2O_3 content (6.37%) was consumed to form hematite and magnetite. The residual Fe_2O_3 would take place in the glassy phase which would be lower than the alkaline and alkaline-earth ratio. Therefore, the glassy phase would have an iron-containing but predominantly alkaline and alkaline-earth aluminosilicate nature. This interpretation was also confirmed by the SEM-EDS analysis of the CFA. The results of the EDS analyses on the selected grains in Figures 5b–5f showed that the amorphous spheres in Figures 5b–1, 5d–3, and 5e–2 were in an Mg-, Na-, and K-aluminosilicate structure. The ferrospheres in Figures 5e–1 and 5f with a dendritic magnetite structure formed on the surface of the amorphous silica and/or Ca-, Mg-, Na-, and K-aluminosilicate spheres as incrustations. Similar structures were also identified by Zhao et al. (2006) and Strzałkowska (2022) in the magnetic fractions of different fly ashes. Strzałkowska (2022) classified the microstructures of ferrospheres based on the decreasing Fe_2O_3 content, which was massive, skeletal, skeletal-dendritic, octahedral, dendritic, and porous. The ferrosphere in Figure 5e–1 had a Fe_2O_3 content of 36.2% (25.35% Fe) according to the results of the semiquantitative SEM-EDS analysis (Table 3), indicating the dendritic structure according to the Strzałkowska (2022) classification. The cluster structure in Figure 5d–2 is composed of Ca-, Mg-, Na-, and K-aluminosilicates. As a result, the presence of iron could not be detected in the semiquantitative SEM-EDS analysis (Table 3) on the amorphous aluminosilicate spheres that were examined. This can be interpreted as Fe being more present in a crystalline form (such as hematite, magnetite).

Thermal treatments (750 °C, 1000 °C, and 1200 °C) applied to the CFA to study the devitrification behavior of the amorphous phase showed that the CFA was sintered at 1200 °C. The sintering temperature of a material depends on its chemical and mineralogical compositions, and some physical properties such as particle size, surface area, and specific gravity. The CFA had small particle sizes and a large surface area, both of which had a positive effect on the sintering process. It also had high SiO_2 and Al_2O_3 contents. These contents formed a high amorphous matrix in which mullite, and quartz crystalline phases were present. Additionally, high $SiO_2+Al_2O_3$ contents caused extra mullite formation from the amorphous matrix of the CFA in the sintering process, which increased the sintering quality (Erol et al., 2008; Acar and Atalay, 2013). In the sintering process, the mullite and hematite contents increased while the quartz content decreased as the sintering temperature was rising. Additionally, the calcite phase and the dolomite phase disappeared at 750 °C and 1000 °C, respectively (Figure 4). The hercynite ($FeAl_2O_4$) phase was also formed at 750 °C, and its relative concentrations increased along with the increasing temperature during the sintering process.

4.2. Elemental mobility
According to the results of the comparisons of the trace element concentrations of the studied CFA to those of the MFA, European, Puertollano, and NBS 1633b (certified) fly ashes (Table 5), almost all trace element concentrations in the CFA were lower than those in the other fly ashes.

The major and trace element concentrations of fly ashes are important with respect to their environmental effect and their usage as raw materials. However, the mobility of these elements under different aquatic conditions, rather than their concentrations, is important in terms of their environmental risk. The obtained results in two different bench dissolution tests (ASTM and TCLP methods) applied on the CFA showed that pH was the most significantly effective parameter in the dissolution process (Figure 6). Figure 6 clearly shows that high pH values (under ASTM test conditions, pH: 10.04) significantly reduced the dissolution ratios, whereas low pH values (TCLP test conditions, pH: 5.13) significantly increased the dissolution ratios. As a result, the pH value decreased in turn, and the dissolution potential of the metals increased. On the contrary, the dissolution potential of the metals decreased with an increase in the pH values (under ASTM test conditions, pH: 10.04). In particular, the dissolution ratios of certain elements (e.g., Zn, Cd) in ash landfills increase significantly if the ambient pH drops below 7.0 (Egemen and Yurteri, 1996). Therefore, the pH of the environment should be kept under control in case of the storage of waste.

The concentrations of the solutions which were extracted from the CFA by two dissolution methods were found to be considerably below the limits set for inert materials in the EU waste acceptance criteria (WAC) for the analyzed elements (Table 6). Within this context, the

Table 5. Trace element concentrations (mg/kg) of the CFA and comparisons to other fly ashes.

Elements	CFA	NBS 1633b certified[a]	MFA[a]	European[b]	Puertollano Spain[b]
Ag	<0.05*	-	-	-	-
As	32	136	40	22–162	140
Ba	150	709	589	311–3134	460
Cd	2	0.8	0.9	1–6	5
Co	<0.05*	50	13	20–112	31
Cr	144	198	44	47–281	108
Cu	90	113	46	39–254	75
Mn	588	-	153	-	511
Mo	<0.05*	-	11	5–22	11
Ni	73	121	22	49–377	96
Pb	<0.05*	68	46	40–175	1075
Sb	<0.05*	6	4	1–120	120
Se	<0.5*	10	6	3–30	7
Sr	282	1041	302	131–4406	131
Zn	138	210	94	70–924	924

-: no data
*: below detection limit of the ICP-OES
[a] From Medina et al., (2010)
[b] From Moreno et al., (2005)

Table 6. ASTM and TCLP dissolution test results for the CFA (mg/kg). Results compared to EU waste acceptance criteria (EUWAC; Council Decision 2003/33/EC) limits for inert, for (stabilized nonreactive hazardous waste) SNRHW, and for hazardous wastes.

Elements	ASTM (mg/kg)	TCLP (mg/kg)	EUWAC Council Decision (2003/33/EC) (mg/kg)		
			Inert	SNRHW	Hazardous
As	0.06	0.02	0.5	2	25
Ba	0.06	0.4	20	100	300
Cd	<0.05*	<0.05*	0.04	1	5
Cr	0.05	0.07	0.5	10	70
Cu	<0.05*	<0.05*	2	50	100
Mo	<0.05*	<0.05*	0.5	10	30
Ni	<0.01*	0.02	0.4	10	40
Pb	<0.05*	<0.05*	0.5	10	50
Sb	<0.05*	<0.05*	0.06	0.7	5
Hg	NA	NA	0.01	0.2	2
Se	<0.5*	<0.5*	0.1	0.5	7
Zn	<0.01*	0.03	4	50	200

*: below detection limit of the ICP-OES
NA: not analyzed

CFA can be classified as inert waste. Due to instrumental difficulties, it was not possible to analyze the presence of Hg. However, since the concentrations of other listed elements were well below the maximum allowable concentrations, this deficiency was not considered to change the evaluation of the CFA as inert waste.

5. Conclusion

In this study, fly ash from the Çatalağzı thermal power plant (CFA), which is the only local bituminous coal-fired power plant in Turkey, was studied. As a result of the physical, chemical, mineralogical, morphological, and thermal characterizations of the CFA, it was concluded that the CFA, a class F fly ash, could be used in many areas such as zeolite synthesis, geomembrane and sinter material production, silica extraction, cement additives, and cenosphere recovery. However, to use it safely, the TCLP test, which is used as a reference method in the use

and disposal of industrial waste, and the ASTM test, were applied to the CFA. The dissolution ratios of the elements were considerably higher in the TCLP test performed under acidic (pH: 5.13) conditions compared to the ASTM test performed in alkaline (pH: 10.04) conditions. The compositions of the TCLP and ASTM solutions of the CFA were far below the limits set for inert materials in the EUWAC. Therefore, the CFA could be classified as inert waste.

Based on the results of both dissolution tests, the most significant parameter that determined the dissolution ratios of the elements was the pH value of the surrounding environment. For this reason, the pH value of the environment should be kept under control in case of the storage of waste. Particularly, the acceptable limits of EUWAC elements should be carefully monitored in landfills.

References

Acar İ (2013). Characterization and utilization potential of class F fly ashes. PhD, Middle East Technical University, Ankara, Turkey, (in English). http://etd.lib.metu.edu.tr/upload/12615688/index.pdf

Acar I, Atalay MU (2013). Characterization of sintered class F fly ashes. Fuel 106: 195–203. https://doi.org/10.1016/j.fuel.2012.10.057

Akar G (2001). Determination of heavy metal contamination resulting from coal ash disposal areas. MSc, Dokuz Eylül University, İzmir, Turkey, (in Turkish).

Akar G, Arslan V, Ipekoglu U, Tekir U (2010). Acid-base production potentials of ash bearing samples from Soma and Yatagan power plants in Turkey. In: XVI International Coal Preparation Congress; Kentucky, USA. pp. 937–946.

Akar G, Polat M, Galecki G, Ipekoglu U (2012). Leaching behavior of selected trace elements in coal fly ash samples from Yenikoy coal-fired power plants, Fuel Processing Technology 104: 50–56. https://doi.10.1016/j.fuproc.2012.06.026

Akar G, Sen S, Yilmaz H, Arslan V, Ipekoğlu U (2013). Characterization of ash deposits from the boiler of Yenikoy coal-fired powerplant, Turkey. International Journal of Coal Geology 105: 85–90. https://doi.org/10.1016/j.coal.2012.12.001

Alvarez-Ayuso E, Querol X, Plana F, Alastuey A, Moreno N et al. (2008). Environmental, physical and structural characterization of geopolymer matrixes synthesized from coal (co-) combustion fly ashes. Journal of Hazardous Materials 154: 175–183. https://doi.10.1016/j.jhazmat.2007.10.008

ASTM American Society for Testing and Materials, D-3987-85 (2004). Standard test method for shake extraction of solid waste with water In Annual Book of ASTM Standards; Section 11: Water and Environmental Technology, ASTM D3987-85.

ASTM C618 (1994). Standard specification for fly ash and raw or calcinated natural pozzolan for use as mineral admixture in Portland cement concrete, American Society for Testing and Materials, Annual Book of ASTM Standards, vol. 04.02, Pennsylvania.

Atabey İİ, Karahan O, Bilim C, Atiş CD (2020). The influence of activator type and quantity on the transport properties of class F fly ash geopolymer. Construction and Building Materials 267: 120–268. https://doi.org/10.1016/j.conbuildmat.2020.120268

Baba A, Gurdal G, Sengunalp F (2010). Leaching characteristics of fly ash from fluidized bed combustion thermal power plant: Case study: Çan (Çanakkale-Turkey). Fuel Processing Technology 91: 1073–1080. https://doi.org/10.1016/j.fuproc.2010.03.015

Baba A, Kaya A (2004). Leaching characteristics of fly ash from thermal power plants of Soma and Tunçbilek, Turkey, Environmental Monitoring Assessment 91: 171–181. https://doi.org/10.1023/B:EMAS.0000009234.42446.d3

Bayat O, (1998). Characterisation of Turkish fly ashes. Fuel 77 (9/10): 1059–1066. https://doi.org/10.1016/S0016-2361(97)00274-3

Bielowicz B, Botor D, Misiak J, Wagner M (2018). Critical elements in Fly ash from the combustion of bituminous coal in major Polish power plants. E3S Web Conferences. 35. https://doi.org/10.1051/e3sconf/20183502003

Çapik M, Yılmaz AO, Çavuşoğlu İ (2012). Present situation and potential role of renewable energy in Turkey. Renewable Energy 46: 1–13. https://doi.org/10.1016/j.renene.2012.02.031

Dai S, Finkelman RB (2018). Coal as a promising source of critical elements: Progress and future prospects International Journal of Coal Geology 186: 155–164. https://doi.org/10.1016/j.coal.2017.06.005

Dai S, Yan X, Ward CR, Hower JC, Zhao L et al. (2016). Valuable elements in Chinese coals: a review. International Geology Review 1–31. https://doi.org/10.1080/00206814.2016.1197802

Dai S, Zhao L, Peng S, Chou CL, Wang X et al. (2010). Abundances and distribution of minerals and elements in high-alumina coal fly ash from the Jungar Power Plant, Inner Mongolia, China. International Journal of Coal Geology 81: 320–332. https://doi.10.1016/j.coal.2009.03.005

Dwivedi A, Jain MA (2014). Fly ash-waste management and overview: A Review. Recent Research in Science and Technology 6: 30–35.

Ecke H, Menad N, Lagerkvist A (2002). Treatment-oriented characterization of dry scrubber residue from municipal solid waste incineration. Journal of Material Cycles and Waste Management 4: 117–126. https://doi.org/10.1007/s10163-001-0063-x

Ediger VŞ, Berk I, Kösebalaban A (2014). Lignite resources of Turkey: Geology, reserves, and exploration history. International Journal of Coal Geology 132: 13–22. https://doi.org/10.1016/j.coal.2014.06.008

Egemen E, Yurteri C (1996). Regulatory leaching tests for fly as: A case study. Waste Management and Research 14 (1): 43–50. https://doi.org/10.1177/0734242X9601400105

El-Naggar MR, El-Kamash AM, El-Dessouky MI, Ghonaim AK (2008). Two-step method to prepare of NaA-X zeolite blend from fly ash for removal of cesium ions. Journal of Hazardous Materials 154: 963–972. https://doi.10.1016/j.jhazmat.2007.10.115

Erol M, Küçükbayrak S, Ersoy-Meriçboyu A (2008). Characterization of sintered coal fly ashes. Fuel 87: 1334–1340. https://doi.10.1016/j.fuel.2007.07.002

EUWAC, EU waste acceptance criteria (EU Council Decision 2003/33/EC) limits: https://eur-lex.europa.eu/legal-content/EN/TXT/PDF/?uri=CELEX:32003D0033&from=GA

EÜAŞ Genel Müdürlüğü Elektrik Üretim Sektör Raporu, (2021) (in Turkish).

Fernandez-Turiel JL, Georgakopoulos A, Gimeno D, Papastergios G, Kolovos N (2004). Ash deposition in a pulverized coal-fired power plant after high-calcium lignite combustion. Energy and Fuels 18: 1512–1518. https://doi.org/10.1021/ef0400161

Font O, Moreno N, Díez S, Querol X, López-Soler A et al. (2009). Differential behavior of combustion and gasification fly ash from Puertollano Power Plants (Spain) for the synthesis of zeolites and silica extraction, Journal of Hazardous Materials 166(1): 94–102. https://doi.10.1016/j.jhazmat.2008.10.120

Franus W, Wiatros-Motyka MM, Wdowin M (2015). Coal fly ash as a resource for rare earth elements. Environmental Science and Pollution Research 22: 9464–9474. https://doi:10.1007/s11356-015-4111-9

Goodarzi F (2006). Characteristics and composition of fly ash from Canadian coal-fired power plants. Fuel: 85 (10–11): 1418–1427. https://doi.org/10.1016/j.fuel.2005.11.022

Haykiri-Acma H, Yaman S, Ozbek N, Kucukbayrak S (2011). Mobilization of some trace elements from ashes of Turkish lignites in rain water, Fuel 90: 3447–3455. https://doi.org/10.1016/j.fuel.2011.06.069

Hower JC, Dai S, Seredin VV, Zhao L, Kostova IJ et al. (2013). A note on the occurrence of yttrium and rare earth elements in coal combustion products. Coal Combustion Gasification Products 5: 39–47. https://doi.4177/CCGP-D-13-00001.1

Hower JC, Groppo JG (2021). Rare Earth-bearing particles in fly ash carbons: examples from the combustion of eastern Kentucky coals. Energy Geoscience 2: 90–98. https://doi.10.1016/j.engeos.2020.09.003

Hower JC, Groppo JG, Henke KR, Graham UM, Hood MM et al. (2017). Ponded and landfilled fly ash as a source of rare earth elements from a Kentucky power plant. Coal Combustion and Gasification Products 9:1–21. https://doi:10.4177/CCGP-D-17-00003.1

Hower JC, Groppo JG, Jewell RF, Wiseman JD, Duvallet TY et al. (2021). Distribution of rare earth elements in the pilot-scale processing of fly ashes derived from eastern Kentucky coals: comparisons of the feed and processed ashes. Fuel 295:120562. https://doi.10.1016/j.fuel.2021.120562

Hower JC, Groppo JG, Joshi P, Preda DV, Gamliel DP et al. (2020). Distribution of Lanthanides, Yttrium, and Scandium in the pilot-scale beneficiation of fly ashes derived from Eastern Kentucky Coals. Minerals 10: 105. https://doi.org/10.1016/j.coal.2022.104015

Hu G, Dam-Johansen K, Wedel S, Hansen JP (2006). Decomposition and oxidation of pyrite. Progress in Energy and Combustion Science 32: 295–314. https://doi.org/10.1016/j.pecs.2005.11.004

Huang Z, Fan M, Tiand H (2018). Coal and coal byproducts: A large and developable unconventional resource for critical materials – rare earth elements. Journal of Rare Earths 36: 337–338. https://doi.org/10.1016/j.jre.2018.01.002

Huang Z, Fan M, Tiand H (2020). Rare Earth elements of fly ash from Wyoming's powder River Basin Coal. Journal of Rare Earths 38: 219–226. https://doi.org/10.1016/j.jre.2019.05.004

Izquierdo M, Querol X (2012). Leaching behaviour of elements from coal combustion fly ash: an overview. International Journal of Coal Geology 94: 54–66. https://doi.org/10.1016/j.coal.2011.10.006

Jankowski J, Ward CR, French D, Groves S (2006). Mobility of trace elements from selected Australian fly ashes and its potential impact on aquatic ecosystems. Fuel 85: 243–256. https://doi:10.1016/j.fuel.2005.05.028

Jegadeesan G, Al-Abed SR, Pinto P (2008). Influence of trace metal distribution on its leachability from coal fly ash. Fuel 87: 1887–1893. https://doi.org/10.1016/j.fuel.2007.12.007

Ji L, Yu H, Zhang R, French D, Grigore M et al. (2019). Effects of fly ash properties on carbonation efficiency in CO_2 mineralisation. Fuel Processing Technology 188: 79–88. https://doi.org/10.1016/j.fuproc.2019.01.015

Karayigit AI, Bulut Y, Querol X, Alastuey A, Vassilev S (2005). Variations in fly ash composition from the soma power plant, Turkey. Energy Sources 27: 1473–1481. https://doi.10.1080/009083190523811

Karayigit AI, Gayer RA, Querol X, Onacak T (2000). Contents of major and trace elements in feed coals from Turkish coal-fired power plants. International Journal of Coal Geology 44: 169–184. https://doi.org/10.1016/S0166-5162(00)00009-4

Karayiğit Aİ, Mastalerz M, Oskay RG, Gayer RA (2018). Coal petrography, mineralogy, elemental compositions and palaeo environmental interpretation of Late Carboniferous coal seams in three wells from the Kozlu coalfield (Zonguldak Basin, NW Turkey). International Journal of Coal Geology 187: 54–70. https://doi.org/10.1016/j.coal.2017.12.007

Karayiğit Aİ, Oskay RG, Gayer RA (2019). Mineralogy and geochemistry of feed coals and combustion residues of the Kangal power plant (Sivas, Turkey). Turkish Journal of Earth Sciences 28: 438–456. https://doi.org/10.3906/yer-1811-7

Karayiğit Aİ, Yiğitler Ö, İşerli S, Querol X, Mastalerz M et al. (2019). Mineralogy and geochemistry of feed coals and combustion residues from Tunçbilek and Seyitömer coal-fired power plants in western Turkey. Coal Combustion and Gasification Products 11: 18–31. https://doi.10.4177/CCGP-D-18-00011.1

Kim A.G, Kazonich G, Dahlberg M (2003). Relative solubility of cations in class F fly ash. Environmental Science & Technology 37: 4507–4511. https://doi.org/10.1021/es0263691

Kizgut S, Cuhadaroglu D, Samanli (2010). Stirred grinding of coal bottom ash to be evaluated as a cement additive. Energy Sources, Part A 32: 1529–1539. https://doi.org/10.1080/15567030902780378

Kolay PK, Bhusal S (2014). Recovery of hollow spherical particles with two different densities from coal fly ash and their characterization. Fuel 117: 118–124. https://doi:10.1016/.j.fuel.2013.09.014

Kolay PK, Singh DN (2001). Physical, chemical, mineralogical, and thermal properties of cenospheres from an ash lagoon. Cement and Concrete Research 31 (4): 539–542. https://doi.org/10.1016/S0008-8846(01)00457-4

Kolker A, Scott C, Hower JC, Jorge A. Vazquez JA et al. (2017). Distribution of rare earth elements in coal combustion fly ash, determined by SHRIMP-RG ion microprobe. International Journal of Coal Geology 184: 1–10. https://doi.org/10.1016/j.coal.2017.10.002

Kopac M, Hilalci A (2007). Effect of ambient temperature on the efficiency of the regenerative and reheat Çatalağzı power plant in Turkey. Applied Thermal Engineering 27: 1377–1385. https://doi.org/10.1016/j.applthermaleng.2006.10.029

Lee WE, Souza GP, McConville CJ, Tarvornpanich T, Iqbal Y (2008). Mullite formation in clays and clay-derived vitreous ceramics. Journal of the European Ceramic Society 28: 465–471. https://doi:10.1016/j.jeurceramsoc.2007.03.009

Lin R, Howard BH, Roth EA, Bank TL, Granite EJ et al. (2017). Enrichment of rare earth elements from coal and coal by-products by physical separations. Fuel 200: 506–520. https://doi.org/10.1016/j.fuel.2017.03.096

Liu F, Liu J, Yu Q, Jin Y, Nie Y (2005). Leaching characteristics of heavy metals in municipal solid waste incinerator fly ash. Journal of Environmental Science and Health, Part A: Toxic/Hazardous Substances and Environmental Engineering 40: 1975–1985. https://doi.org/10.1080/10934520500184707

Lu SG, Chen YY, Shan HD, Bai SQ (2009). Mineralogy and heavy metal leachability of magnetic fractions separated from some Chinese coal fly ashes. Journal of Hazardous Materials 169: 246–255. https://doi.org/10.1016/j.jhazmat.2009.03.078

Manz OE (1999). Coal fly ash: a retrospective and future look. Fuel 78: 133–136 https://doi.org/10.1016/S0016-2361(98)00148-3

Medina A, Gamero P, Querol X, Moreno N, DeLeón B et al. (2010). Fly ash from a Mexican mineral coal I: Mineralogical and chemical characterization. Journal of Hazardous Materials 181: 82–90. https://doi.10.1016/j.jhazmat.2010.04.096

Moreno N, Querol X, Plana F, Alastuey A, Janssen M et al. (2002). Zeolite synthesis from pure silica extracted from coal fly ashes. Journal of Chemical Technology and Biotechnology 268–2575. https://doi.10.1002/jctb.578

Moreno N, Querol X, Andres JM, Stanton K, Towler M et al. (2005). Physico-chemical characteristics of European pulverized coal combustion fly ashes. Fuel 84: 1351–1363. https://doi.org/10.1016/j.fuel.2004.06.038

Oskay RG, Inaner H, Karayigit AI, Christanis K (2013). Coal deposits of Turkey: properties and importance on energy demand. Bulletin of Geological Society of Greece 47: 2111–2120. https://doi.10.12681/bgsg.11106

Panitchakarn P, Laosiripojana N, Viriya-umpikul N, Pavasant P (2014). Synthesis of high-purity Na-A and Na-X zeolite from coal fly ash. Journal of the Air & Waste Management Association 64 (5): 586–596. https://doi.10.1080/10962247.2013.859184

Perkin Elmer Handbook (1976). Analytical methods for atomic absorption spectrophotometry, Perkin-Elmer Corporation USA.

Querol X, Moreno N, Umaña JC, Alastuey A, Hernández E et al. (2002). Synthesis of zeolites from coal fly ash: an overview. International Journal of Coal Geology 50: 413–423. https://doi.S0166-5162(02)00124-6

Querol X, Umaña JC, Plana F, Alastuey A, Lopez-Soler A et al. (2001). Synthesis of zeolites from fly ash at pilot plant scale. Examples of potential applications. Fuel 80: 857–865. https://doi.10.1016/S0016-2361(00)00156-3

Roy R, Das D, Kumar Rout P (2022). A Review of advanced mullite ceramics. Engineered Science 18: 20–30. https://doi.10.30919/es8d582

Rybak A, Rybak A (2021). Characteristics of some selected methods of rare Earth elements recovery from coal fly ashes. Metals 11: 142. https://doi.org/10.3390/met11010142 10.3390/met110101

Seredin VV, Dai S (2012). Coal deposits as potential alternative sources for lanthanides and yttrium. International Journal of Coal Geology 94: 67–93. https://doi.org/10.1016/j.coal.2011.11.001

Seyrek E (2018). Engineering behavior of clay soils stabilized with class C and class F fly ashes. Science and Engineering of Composite Materials 25: 273–287. https://doi.org/10.1515/secm-2016-0084

Spears DA (2000). Role of clay minerals in UK coal combustion. Applied Clay Science 16: 87–95. https://doi.org/10.1016/S0169-1317(99)00048-4

Spears DA (2004). The use of laser ablation inductively coupled plasma-mass spectrometry (LA ICP-MS) for the analysis of fly ash. Fuel 83: 1765–1770. https://doi:10.1016/j.fuel.2004.02.018

Strzałkowska E (2021). Morphology, chemical and mineralogical composition of magnetic fraction of coal fly ash. International Journal of Coal Geology 240: 103746. https://doi.org/10.1016/j.coal.2021.103746

Strzałkowska E (2022). Rare Earth elements and other critical elements in the magnetic fraction of fly ash from several Polish power plants. International Journal of Coal Geology 258: 104015. https://doi.org/10.1016/j.coal.2022.104015

Strzałkowska E, Adamczyk Z (2019). Influence of chemical composition of fy-ash cenospheres on their grains size. International Journal of Environmental Science and Technology 17: 809–818. https://doi.org/10.1007/s13762-019-02512-2

Stuckman MY, Lopano CL, Granite EJ (2018). Distribution and speciation of rare earth elements in coal combustion by-products via synchrotron microscopy and spectroscopy. International Journal of Coal Geology 195: 125–138. https://doi.org/10.1016/j.coal.2018.06.001

Sultana P, Das S, Bagchi B, Bhattacharya A, Basu R et al. (2011). Effect of size of fly ash particle on enhancement of mullite content and glass formation. Bulletin Material Science 34 (7): 1663–1670. https://doi.org/10.1007/s12034-011-0374-z

Tanriverdi M, Akar Şen G, Çiçek T, Şen S, Önel Ö (2021). Leachability of heavy metals from autoclaved fly ash-lime building bricks. Journal of the Polish Mineral Engineering Society 1 (1): 67–74. https://doi.org/10.29227/IM-2021-01-09

Top S, Vapur H (2020). Zeolite synthesis by alkali fusion method using two different fly ashes derived from Turkish thermal power plants. Scientific Mining Journal 59 (1): 7–14. http://www.mining.org.tr/en/download/article-file/1011040

Ugurlu A (2004). Leaching characteristics of fly ash. Environmental Geology 46: 890–895. https://doi.org/10.1007/s00254-004-1100-6

USEPA United States Environmental Protection Agency Test Method 1311-TCLP, Toxicity characteristic leaching procedure 1992. Washington, DC. 35pp.

Vassilev SV, Menendez R, Borrego AG, Diaz-Somoano M, Martinez-Tarazona MR (2004). Phase-mineral and chemical composition of coal fly ashes as a basis for their multicomponent utilization. 3. Characterization of magnetic and char concentrates. Fuel 83: 1563–1583. https://doi.org/10.1016/j.fuel.2004.01.010

Vassilev SV, Vassileva CG, Karayigit AI, Bulut Y, Alastuey A et al. (2005). Phase-mineral and chemical composition of composite samples from feed coals, bottom ashes and fly ashes at the Soma power station, Turkey. International Journal of Coal Geology 61 (1–2): 35–63. https://doi.org/10.1016/j.coal.2004.06.004

Veeresh H, Tripathy S, Chaudhuri D, Ghosh BC, Hart BR et al. (2003). Changes in physical and chemical properties of three soil types in India as a result of amendment with fly ash and sewage sludge. Environmental Geology 43: 513–520 https://doi.10.1007/s00254-002-0656-2

Wang Z, Dai S, Zou J, French D, Graham IT (2019). Rare earth elements and yttrium in coal ash from the Luzhou power plant in Sichuan, Southwest China: Concentration, characterization and optimized extraction. International Journal of Coal Geology 203: 1–14. https://doi.org/10.1016/j.coal.2019.01.001

Wong JWC (1995). The production of artificial soil mix from coal fly ash and sewage sludge. Environmental Technology 16 (8): 741–751. https://doi.10.1080/09593331608616313

Yadav VK, Fulekar MH (2020). Advances in methods for recovery of ferrous, alumina, and silica nanoparticles from fly ash waste. Ceramics 3 (3): 384–420. https://doi.org/10.3390/ceramics3030034

Yildirim H, Sümer M, Akyüncü V, Gürbüz E (2011). Comparison on efficiency factors of F and C types of fly ashes. Construction and Building Materials 25: 2939–2947. https://doi.org/10.1016/j.conbuildmat.2010.12.009

Yılmaz H (2015). Characterization and comparison of leaching behaviors of fly ash samples from three different power plants in Turkey. Fuel Processing Technology 137: 240–249. https://doi.org/10.1016/j.fuproc.2015.04.011

Yilmaz MS, Karamahmut Mermer N (2016). Conversion of fly ashes from different regions to mesoporous silica: effect of the mineralogical composition. Journal of Sol-Gel Science and Technology 78: 239–247. https://doi.10.1007/s10971-016-3963-x

Zandi M, Russell NV (2007). Design of a leaching test framework for coal fly ash accounting for environmental conditions. Environmental Monitoring Assessment 131: 509–526. https://doi.10.1007/s10661-006-9496-y

Żelazny S, Świder H, Jarosiński A, Białecka B (2020). The recovery of rare-earth metals from fly ash using alkali pre-treatment with sodium hydroxide. Mineral Resources Management 36 (3): 127–144. https://doi.10.24425/gsm.2020.133930

Zhao Y, Zhang J, Sun J, Bai X, Zheng C (2006). Mineralogy, chemical composition, and microstructure of ferrospheres in fly ashes from coal combustion. Energy and Fuels 20: 1490–1497. https://doi.org/10.1021/ef060008f

Żyrkowski M, Neto RC, Santos LF, Witkowski K (2016). Characterization of fly-ash cenospheres from coal-fired power plant unit. Fuel 174: 49–53. https://doi.org/10.1016/j.fuel.2016.01.061